Calorimetric study of smectic polymorphism in octyloxyphenyl-nitrobenzoyloxy benzoate + decyloxyphenyl-nitrobenzoyloxy benzoate mixtures

K. Ema,* G. Nounesis, and C. W. Garland
Department of Chemistry, Massachusetts Institute of Technology, Cambridge, Massachusetts 02139

R. Shashidhar
Raman Research Institute, Bangalore 560 080, India

(Received 1 September 1988)

Binary mixtures of octyloxyphenyl-nitrobenzoyloxy benzoate (DB_8ONO_2) and decycloxyphenyl-nitrobenzoyloxy benzoate ($DB_{10}ONO_2$) exhibit a rich variety of smectic polymorphism. An ac calorimetric study has been carried out on six mixtures with mole percent X of the decyl homolog between 51 and 57, a range that includes the Sm-A_d–N_r–Sm-A_1 point at $X \simeq 56$. The sample with $X = 57$ exhibits a first-order direct Sm-A_d–Sm-A_1 transition, while the sample with $X = 51.3$ exhibits two transitions—a second-order Sm-A_d–N_r transition with a very small excess heat-capacity peak and a tricritical N_r–Sm-A_1 transition with a large heat-capacity peak. For samples with intermediate compositions, only weakly first-order N_r–Sm-A_1 heat-capacity peaks are observed in the vicinity of the Sm-A_d–N_r–Sm-A_1 point. All six investigated samples exhibit the Sm-A_1–Sm-$\tilde{C}$–Sm-C_2 phase sequence at lower temperatures. The Sm-A_1–Sm-$\tilde{C}$ transition is a weakly first-order phase transition with pretransitional excess heat capacity below the transition temperature. In contrast, the Sm-$\tilde{C}$–Sm-C_2 transition is a weakly first-order inverted Landau transition with no pretransitional behavior in the Sm-C_2 phase below the transition but a large mean-field excess heat capacity observed in the Sm-$\tilde{C}$ phase above the transition.

I. INTRODUCTION

Recent theoretical[1–7] and experimental[8–14] work has established a rich variety of smectic polymorphism for liquid-crystal molecules with a long (three-ring) aromatic core and a strongly polar end group. This polymorphism and associated reentrant behavior, which is the result of frustration arising from the presence of two distinct length scales,[1,2] is well illustrated by 4-alkoxyphenyl-4′-nitrobenzoyloxy benzoate:

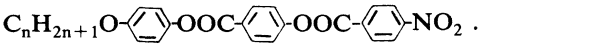

This homologous series of compounds has been denoted as DB_nONO_2 or $DB.\bar{n}.NO_2$, and we shall use the former designation.

Pure DB_9ONO_2 exhibits the following sequence of phase transitions on cooling at atmospheric pressure:[10]

$$I \xrightarrow[497\ \mathrm{K}]{} N \xrightarrow[468\ \mathrm{K}]{} \text{Sm-}A_d \xrightarrow[429\ \mathrm{K}]{} N_r \xrightarrow[411.6\ \mathrm{K}]{} \text{Sm-}A_{d,r} \xrightarrow[397\ \mathrm{K}]{} N_r \xrightarrow[394.6\ \mathrm{K}]{} \text{Sm-}A_1 \xrightarrow[392\ \mathrm{K}]{} \text{Sm-}\tilde{C} \xrightarrow[373\ \mathrm{K}]{} \text{Sm-}A_2 \xrightarrow[369\ \mathrm{K}]{} \text{Sm-}C_2 \ .$$

The symbols I and N denote the isotropic and nematic phases, and the symbols Sm-A and Sm-C denote smectic-A (where the director is normal to the smectic layers) and smectic-C (where the director is tilted with respect to the layer normal) phases. The subscript r indicates a reentrant phase. For the smectic phases, Sm-A_d is a partial bilayer for which $L < d < 2L$, where d is the layer thickness and L is the length of a molecule, Sm-A_1 is a monolayer smectic-A phase with $d \simeq L$, Sm-A_2 is a bilayer smectic-A phase with $d \simeq 2L$, Sm-C_2 is a tilted bilayer, and Sm-$\tilde{C}$ is a fluid antiphase with a periodic polarization modulation that is tilted with respect to the smectic layers.[8]

The stability of the N_r and Sm-A_d phases is sensitive to composition as shown in Fig. 1. This figure presents the overall phase diagram for binary mixtures of the two homologs DB_8ONO_2 and $DB_{10}ONO_2$.[14] Much of the earlier work on related polar systems was focused primarily on the N and A_d reentrant behavior and on N–Sm-A_1 transitions that occur far from the Sm-A_d–N_r–Sm-A_1 point.[15,16] The present work concerns N_r-A_1 transitions near the Sm-A_d–N_r–Sm-A_1 point and the lower temperature Sm-A_1–Sm-$\tilde{C}$ and Sm-$\tilde{C}$–Sm-A_2–Sm-C_2 transitions. The simplest description of the Sm-A_d–N_r–Sm-A_1 point is a bicritical point where second-order Sm-A_d–N_r and N_r–Sm-A_1 phase boundaries meet a first-order Sm-A_d–Sm-A_1 line. This is directly analogous to a magnetic bicritical point. However, if both the Sm-A_d–N_r and N_r–Sm-A_1 transitions are second order and belong to the XY universality class, this

multicritical point is expected to be a tetracritical point rather than a bicritical point.[3,4] A recent high-resolution phase diagram for $DB_8ONO_2+DB_{10}ONO_2$ mixtures[14] shows that the topology near the Sm-A_d–N_r–Sm-A_1 point does not conform to the expected bicritical or tetracritical topology. Furthermore, very detailed differential scanning calorimetry (DSC) data[14] suggest that the N_r–Sm-A_1 transition becomes first order close to the Sm-A_d–N_r–Sm-A_1 point. In this case, the "multicritical point" splits into a critical end point for the second-order Sm-A_d–N_r line and a tricritical point along the N_r–Sm-A_1 transition line. Very recent theoretical results[4] support this topology as an alternative possibility.

In the present work we have used an ac calorimetric technique to investigate several $DB_8ONO_2+DB_{10}ONO_2$ mixtures. The objectives are to (a) determine the character of the N_r–Sm-A_1 transition as the composition approaches that of the Sm-A_d–N_r–Sm-A_1 point and (b) provide a detailed view of the heat-capacity variation in the vicinity of the Sm-A_1–Sm-$\tilde{C}$ and Sm-$\tilde{C}$–Sm-A_2–Sm-C_2 transitions.

II. RESULTS

The investigated mixtures of $DB_8ONO_2+DB_{10}ONO_2$ were prepared at the Raman Research Institute from compounds synthesized at the Technical University of Berlin. Calorimetric measurements were made at MIT using a high-resolution ac technique that has been described previously.[17] A small quantity ($\sim$60 mg) of each mixture was hermetically sealed in a silver sample cell using a cold-welded tin seal. This prevents contact between the liquid crystal and the ambient atmosphere. The observed transition temperatures were stable except for N_r–Sm-A_1 transitions near the Sm-A_d–N_r–Sm-A_1 point, a feature that will be discussed later.

The overall temperature dependence of the specific-heat capacity C_p is shown over a wide temperature range in Figs. 2 and 3 for two typical samples with $X=51.33$ and 54.2, respectively, where X is the mole percent of $DB_{10}ONO_2$ in the mixture. These C_p values were obtained from

$$C_p=(C_p^{(\mathrm{obs})}-C_p^{(\mathrm{empty})})/m\ , \tag{1}$$

where $C_p^{(\mathrm{obs})}$ is the observed heat capacity of the filled cell, $C_p^{(\mathrm{empty})}$ is that of the empty cell, and m is the mass of the liquid-crystal sample in grams. The value of $C_p^{(\mathrm{empty})}$ is almost constant, exhibiting a small linear temperature dependence throughout the investigated temperature range.

The points in Figs. 2 and 3 marked by crosses are data points for which the phase shift ϕ of the oscillating T_{ac} signal had anomalously high values, indicating the coexistence of two phases at a first-order transition.[17] For all investigated mixtures, the Sm-A_1–Sm-$\tilde{C}$ transition was weakly first order. The heat-capacity data indicate only a single transition in the Sm-$\tilde{C}$–Sm-A_2–Sm-C_2 region, and microscopic examination of the samples did not show clear evidence of a Sm-A_2 phase. Thus we interpret the single large C_p peak at $\sim$373 K as due to a direct Sm-$\tilde{C}$–Sm-C_2 transition. This Sm-$\tilde{C}$–Sm-C_2 transition was clearly first order but exhibited a large pretransitional heat capacity in the high-temperature Sm-$\tilde{C}$ phase.

Six samples with X values of 51.33, 53.2, 54.2, 55.0, 55.25, and 57.0 were investigated over the temperature range from 375 to 405 K. This region of the phase diagram corresponds to the dashed rectangle in Fig. 1. The phase transition temperatures determined calorimetrically are shown in Fig. 4(a). A detailed view of the Sm-

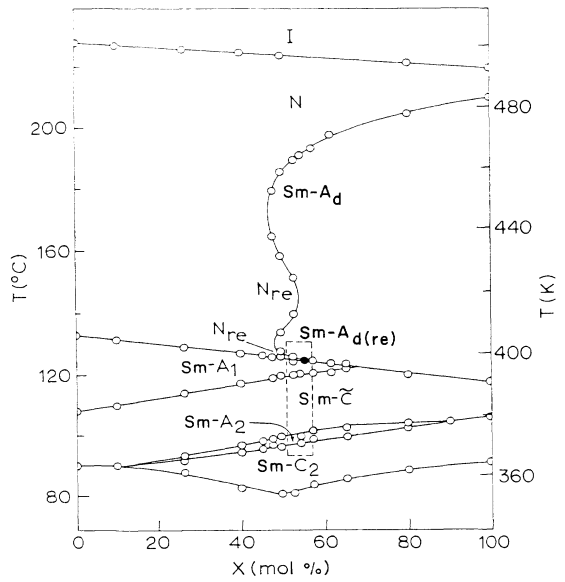

FIG. 1. Phase diagram for $DB_8ONO+DB_{10}ONO_2$ mixtures as given in Ref. 14. X denotes the mole percent of $DB_{10}ONO_2$. The region studied in the present investigation is indicated by the dashed rectangle.

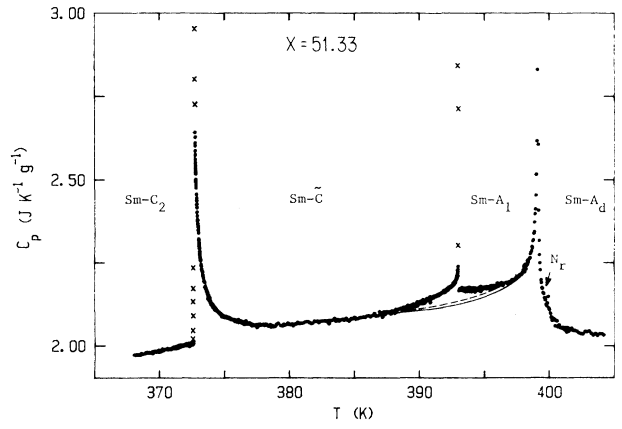

FIG. 2. Specific-heat capacity of a $DB_8ONO_2+DB_{10}ONO_2$ mixture containing 51.33 mol % $DB_{10}ONO_2$. The points denoted by crosses indicate the coexistence of two phases at the Sm-A_1–Sm-$\tilde{C}$ and Sm-$\tilde{C}$–Sm-C_2 transitions. A very small C_p peak at the Sm-A_d–N_r transition is shown clearly in Fig. 7. The solid and dashed curves in the vicinity of the Sm-A_1–Sm-$\tilde{C}$ transition represent an estimated lower and upper bound for the "background" heat capacity in this region.

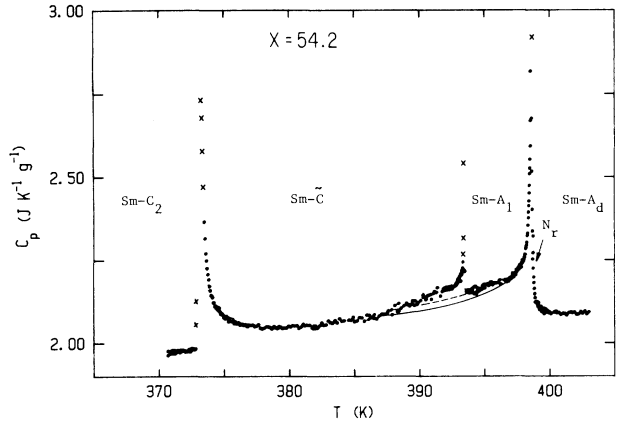

FIG. 3. Specific-heat capacity of a $DB_8ONO_2+D_{10}ONO_2$ mixture containing 54.2 mol% $DB_{10}ONO_2$. See the legend of Fig. 2 for further details. In this sample, no heat-capacity anomaly was observed at the Sm-A_d–N_r transition (see Fig. 8).

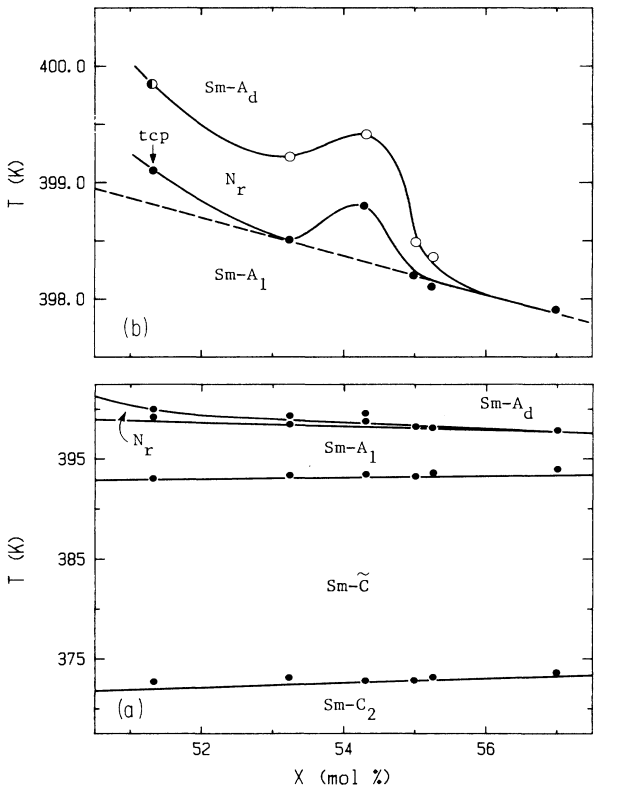

FIG. 4. Partial phase diagram of $DB_8ONO_2+DB_{10}ONO_2$ mixtures: (a) the region studied in this work, (b) a detailed view of the Sm-A_d–N_r–Sm-A_1 region. The phase lines in (a) were taken from Fig. 1; the Sm-$\tilde{C}$–Sm-C_2 line corresponds to the Sm-A_2–Sm-C_2 line in Fig. 1. The lines in (b) are merely estimates of the phase boundaries in this narrow temperature range since there is considerable uncertainty about some of the transition temperatures; see text. The closed circles indicate transition temperatures obtained calorimetrically, and the open circles indicate Sm-A_d–N_r temperatures observed microscopically. The dashed line in (b) represents the N_r–Sm-A_1 and Sm-A_d–Sm-A_1 line from Fig. 1 shifted up 0.7 K.

A_d–N_r–Sm-A_1 region, showing both calorimetric transition temperatures and microscopic Sm-A_d–N_r temperatures, is given in Fig. 4(b).

Figure 5 shows the variation of C_p and the phase shift ϕ for the Sm-$\tilde{C}$–Sm-C_2 transition region in the sample with $X=51.33$. A coexistence range of 170 mK is clearly indicated by the abrupt increase in ϕ, which is constant over a wide temperature range away from the transition. The heat-capacity variation associated with the Sm-$\tilde{C}$–Sm-C_2 transition in all the other investigated samples is very similar to that shown in Fig. 5. However, the width of the coexistence region increases slowly as the concentration of $DB_{10}ONO_2$ is increased, reaching 350 mK for $X=55.25$ and 400 mK for $X=57.0$. An analysis of the C_p data for the Sm-$\tilde{C}$–Sm-C_2 transition in terms of a Landau model is given in Sec. III.

Typical C_p variations observed near the Sm-A_1–Sm-$\tilde{C}$ transition are shown in detail in Fig. 6 for mixtures with $X=51.33$ and 54.2. The solid and dashed curves represent estimates of the "background" heat capacity in the Sm-A_1–Sm-$\tilde{C}$ region. In each case, these lines correspond to those given in Figs. 2 and 3. Heat-capacity data points that are artificially high due to the coexistence of two phases (indicated by crosses in Figs. 2 and 3) are not shown. The Sm-A_1–Sm-$\tilde{C}$ coexistence range is 60 mK for $X=51.33$ and 200 mK for $X=54.2$. There was no systematic trend in the width of the coexistence range as a function of X; the values for other mixtures lie between 125 and 250 mK.

The variation in the heat capacity of the 51.33 mol% mixture was studied at a slow scanning rate in the Sm-A_d–N_r–Sm-A_1 region, and the results are shown in Fig. 7. There were no changes in the size and shape of the C_p peaks observed on three runs extending over a period of

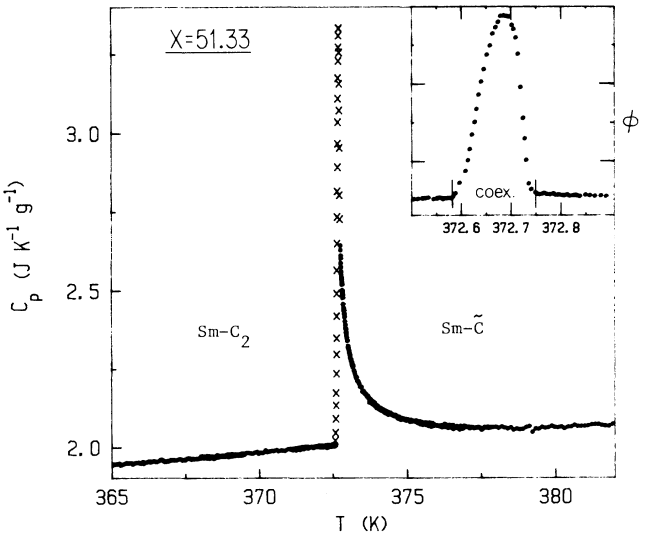

FIG. 5. Variation of C_p in the vicinity of the Sm-$\tilde{C}$–Sm-C_2 transition for the mixture with $X=51.33$. As in Fig. 2, the crosses indicate artificial C_p values observed when two phases coexist. The coexistence region is clearly indicated by the abrupt increase in the phase shift ϕ shown in the inset.

50 h. The only change was a small shift in the positions of the peaks: the drift rate dT_c/dt was -1.4 mK/h for the Sm-A_d-N_r transition and -0.8 mK/h for the N_r-Sm-A_1 transition. Note the very small magnitude of the C_p peak associated with the Sm-A_d-N_r transition in this sample. No thermal anomaly could be observed at the Sm-A_d-N_r transition for any of the other samples.

A comparison of the C_p variation in the Sm-A_d-N_r-Sm-A_1 region for several mixtures is given in Fig. 8. Except for the case of the stable 51.33 mol% mixture, high-resolution heat-capacity data were difficult to obtain in this region since the C_p peaks drifted quite rapidly toward lower temperatures. The behavior of the 57.0 mol% mixture was straightforward. This sample exhibited a first-order Sm-A_d-Sm-A_1 transition with a coexistence region 500-mK wide. The drift rate for the transition temperature was -6 mK/h, and the shape of the pretransitional C_p wings did not change with time. The magnitude of the pretransitional excess C_p is too small to see easily on the scale used in Fig. 8, but it is present in the Sm-A_1 phase over ~ 3 K and to a smaller extent in the Sm-A_d phase over ~ 2 K. For the samples with $53.2 \leq X \leq 55.25$, the shape and position (T_{max}) of the C_p(N_r-Sm-A_1) peak changed appreciably as a function of time (drift rates ranged from -30 to -100 mK/h). The C_p data shown in Fig. 8 are in each case those measured early during the first run on the sample. No data are shown for the 53.2 and 55.25 mol% samples

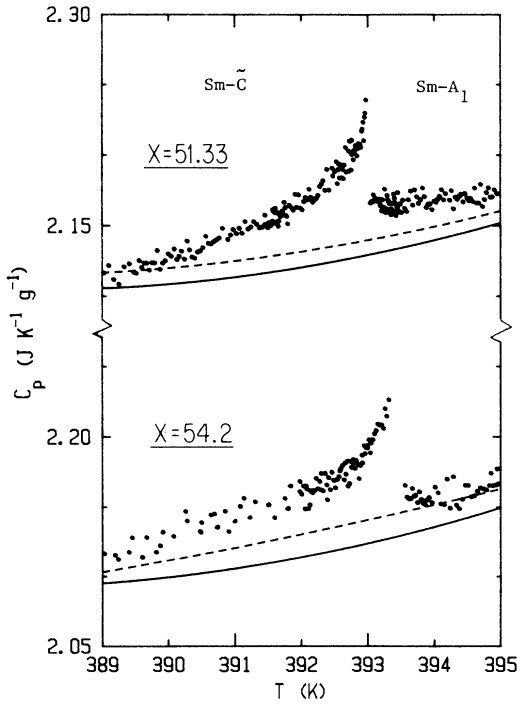

FIG. 6. Detailed view of the C_p variation near the Sm-A_1-Sm-$\tilde{C}$ transition in samples with $X = 51.33$ and 54.2. The solid and dashed curves represent the background curves shown in Figs. 2 and 3. Both these transitions are weakly first order, and data points in the narrow coexistence region are not shown.

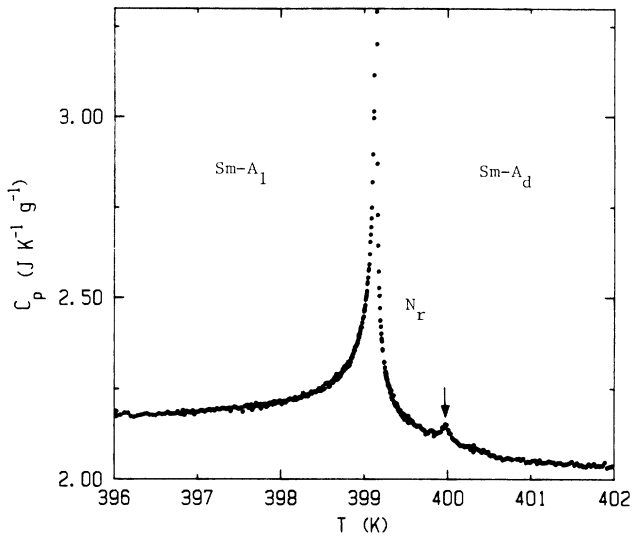

FIG. 7. The C_p variation in the Sm-A_d-N_r-Sm-A_1 transition region for the 51.33 mol% mixture. Note the very small Sm-A_d-N_r peak marked by the arrow. These data were obtained on a slow heating run (scan rate $= +95$ mK/h).

since the initial C_p(N_r-Sm-A_1) peak was already substantially shifted and distorted in these samples by the time the Sm-A_d-N_r-Sm-A_1 region was investigated. The N_r-Sm-A_1 transition temperatures in Fig. 4 correspond to "zero-time" values obtained by using the measured drift rates to correct for the length of time each sample had spent at high temperature prior to reaching

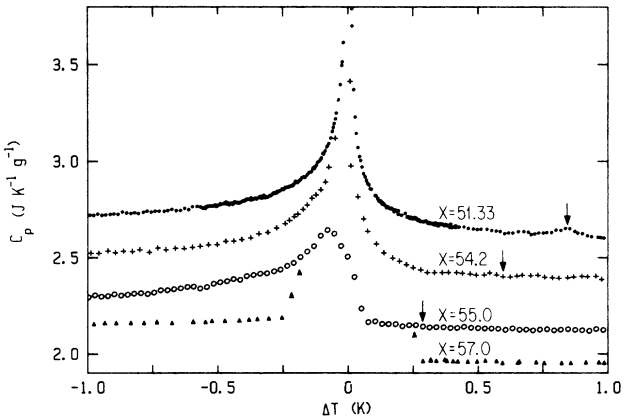

FIG. 8. Detailed view of the C_p variation associated with the N_r-Sm-A_1 transition ($X = 51.33$, 54.2, and 55.0) and the direct first-order Sm-A_d-Sm-A_1 transition ($X = 57.0$). The data for $X = 55.0$, 54.2, and 51.33 have been shifted by $+0.1$, $+0.3$, and $+0.5$ J K^{-1} g^{-1}, respectively. The arrows mark the Sm-A_d-N_r transition observed for the 51.33 mol% sample and the position expected for the 54.2 and 55.0 mol% samples on the basis of microscope observations. In order to avoid confusion, only three data points in the two-phase coexistence region are shown for the 57.0 mol% sample. The transition temperatures used to determine ΔT were $T_c = 339.14$ K (51.33 mol%), $T_1 = 398.80$ K (54.2 mol%), 398.20 K (55.0 mol%), and 397.85 K (57.0 mol%).

the $C_p(N_r\text{-Sm-}A_1)$ maximum on the first run. No such corrections are needed for the Sm-A_1–Sm-$\tilde{C}$ or Sm-$\tilde{C}$–Sm-C_2 transition temperatures since the drift rates are small (-2 to $+2$ mK/h) for these transitions.

The evolution of the heat-capacity peaks in the Sm-A_d–N_r–Sm-A_1 region as a function of time is shown in Fig. 9 for the 51.33 mol% sample. This was the only sample for which the N_r–Sm-A_1 drift rate was slow enough to permit a detailed study without complications due to overlap between the N_r–Sm-A_1 and Sm-A_1–Sm-$\tilde{C}$ transitions. Indeed, this sample was very stable over three runs made under normal operating conditions where T_{max} was 405 K and the temperature exceeded 400 K only for short periods. Following run 3, the sample was held at 415 K for a long time (84 h) in order to induce some decomposition so that the effects of thermally generated impurities could be studied. The C_p variations observed in runs 4–9 are shown in Fig. 9, and the accumulated length of time that the sample was above 400 K prior to each run is indicated. Note that the shape and size of the N_r–Sm-A_1 peak remains almost unchanged but the subsidiary Sm-A_d–N_r peak becomes sharper and the N_r range decreases from run 4 to run 6. The N_r–Sm-A_1 transition was weakly first order for runs 4–7, as evidenced by the observation of anomalous phase shifts ϕ associated with the data points near the maximum in C_p and also by a systematic distortion in the shape of the $C_p(N_r\text{-Sm-}A_1)$ peak observed in run 7. The N_r–Sm-A_1 coexistence region varied from 40 mK in run 4 to 67 mK in run 7. When the N_r phase disappeared, the Sm-A_d–Sm-A_1 transition becomes more strongly first order and the coexistence region was large (110 and 136 mK in runs 8 and 9, respectively). The C_p (and ϕ) data for run 9 are qualitatively like those observed for the 57.0 mol% sample, except that the latter is even more strongly first order and has a wider coexistence region.

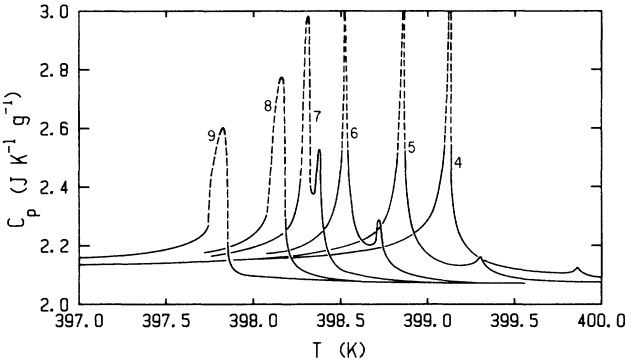

FIG. 9. The evolution of the heat capacity of the 51.33 mol% mixture in the Sm-A_d–N_r–Sm-A_1 region as a function of elapsed time. Run numbers are given; these runs were made following completion of three runs carried out under normal operating conditions (see text). The accumulated time *above* 400 K at the beginning of each run is (4) 86 h, (5) 126 h, (6) 167 h, (7) 193 h, (8) 206 h, and (9) 219 h. The dashed portions of curves indicate apparent C_p values obtained in a two-phase coexistence region.

III. DISCUSSION

Sm-$\tilde{C}$–Sm-C_2 transition. The structure of the Sm-$\tilde{C}$ phase, shown very schematically in Fig. 10, is rather unusual in that the mass-density ordering is almost the same as in a smectic-A phase.[11–13] There is a regular pattern of Sm-A_2-like head-to-head polar ordering as in the Sm-$\tilde{A}$ fluid antiphase, but unlike that phase the polarization unit cell is tilted in the Sm-$\tilde{C}$ phase. One can easily see how Sm-$\tilde{C}$ might transform into Sm-C_2 via the two-step process Sm-$\tilde{C}\rightarrow$Sm-$A_2\rightarrow$Sm-C_2 observed microscopically in Ref. 14. First, the dimer pairs could permeate perpendicular to the smectic mass-density layers to form a Sm-A_2 structure; then a Sm-A_2–Sm-C_2 tilt of the molecular axes with respect to the layer normal would occur.[18] However, the observation of a narrow Sm-A_2 range is sensitive to sample handling even for rapid microscopic scans, and samples exhibiting a Sm-A_2 phase on the initial run may show a direct Sm-$\tilde{C}$–Sm-C_2 transition on subsequent runs. In any event, the point of importance here is the fact that the Sm-$\tilde{C}$–Sm-C_2 transition involves both long-range polarization ordering and a Sm-A–Sm-C type of molecular axis tilt.

Empirically, we find that the heat-capacity variation associated with the Sm-$\tilde{C}$–Sm-C_2 transition can be well described by an inverted Landau form

$$C_p=\begin{cases}C_{p0}+\Delta C_p, & T<T_1 \quad (2a)\\ C_{p0}+A^*(T-T_k)^{-1/2}, & T>T_1>T_k \quad (2b)\end{cases}$$

where T_1 is a first-order transition temperature located somewhere in the coexistence region. The quantity C_{p0} represents the "regular" background heat-capacity variation, and it is given by $B+E\Delta T$ where $\Delta T=T-T_1$. Fits with this inverted Landau form are shown for the 51.33 and 55.25 mol% samples in Figs. 11 and 12. The least-squares fitting parameters are given in Table I. Other samples gave the same type of Sm-$\tilde{C}$–Sm-C_2 behavior.

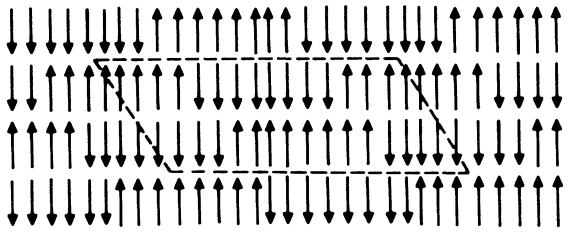

FIG. 10. A highly simplified schematic model of the smectic-$\tilde{C}$ structure. A very small tilt of the director with respect to the layer normal has been ignored; this angle is much smaller than that typically seen in Sm-C_2 phases. The arrows indicate the polar end groups. Note that the *local* polar ordering is predominantly Sm-A_2-like, but the polarization modulation is tilted with respect to the molecular layers. The oblique centered Sm-$\tilde{C}$ lattice can be considered as a "sheared" variant of the Sm-$\tilde{A}$ structure.

Indeed, the 53.2, 54.2, and 55.0 mol % samples exhibit C_p variations that are almost identical to that shown in Fig. 11. The 57.0 mol % sample heat capacity is close to that shown in Fig. 12 except for the small nonlinearity just below the transition. This feature was reproducible for the 55.25 mol % sample but was not seen in any other sample.

Equation (2) can be derived for a first-order Sm-$\tilde{C}$–Sm-A_2, SmA_2–Sm-C_2 transition sequence from the following free-energy form:

$$G=\begin{cases} G_1(T), & T<T_1^* \quad (3a)\\ G_0(T), & T_1^*<T<T_1 \quad (3b)\\ G_0(T)+a\dfrac{T_0-T}{T_0}(\psi_2-\psi)^2+b(\psi_2-\psi)^4+c(\psi_2-\psi)^6, & T>T_1 \quad (3c)\end{cases}$$

where $a,c>0$, and $G_0(T)=G_1(T)$ but $C_{p0}\neq C_{p1}$ at $T=T_1^*$. The polarization order parameter ψ has a saturation value ψ_2, which pertains below T_1, and Eq. (3c) represents an expansion about an ordered Sm-A_2 phase. It is assumed that the smectic molecular axis tilt undergoes a simplified Sm-A_2–Sm-C_2–type transition at T_1^*, very close to T_1. The quantity

$$C_{p1}=-T(\partial^2 G_1/\partial T^2)$$

is the heat capacity in the fully ordered Sm-C_2 phase that exists below T_1^*. The quantity

$$C_{p0}=-T(\partial^2 G_0/\partial T^2)$$

is the heat capacity of a Sm-A_2 phase (hypothetical in our experimental system) that would exist in the narrow range T_1 to T_1^*.

Equation (2b) follows directly from Eqs. (3b) and (3c) with A^* and T_k defined by[19]

$$A^*\equiv\frac{a^{3/2}}{(12cT_0)^{1/2}},\quad T_k\equiv T_0-\frac{b^2T_0}{3ac}\ . \quad (4)$$

If $b<0$, a first-order transition will occur at T_1, where

$$T_1=T_0-\frac{b^2T_0}{4ac}>T_k\ . \quad (5)$$

The heat-capacity step $\Delta C_p=C_{p1}-C_{p0}$ at T_1^* arising from Eqs. (3a) and (3b) is a simplified but excellent approximation for the experimentally observed C_p behavior at a Sm-A_2–Sm-C_2 phase transition.[20] If $T_1=T_1^*$ (Sm-A_2 range is zero) or $T_1-T_1^*$ is small compared to the observed width of the coexistence range (170–400 mK in the present cases), the two mean-field transitions will merge into a single transition described outside the coexistence range by Eq. (2).

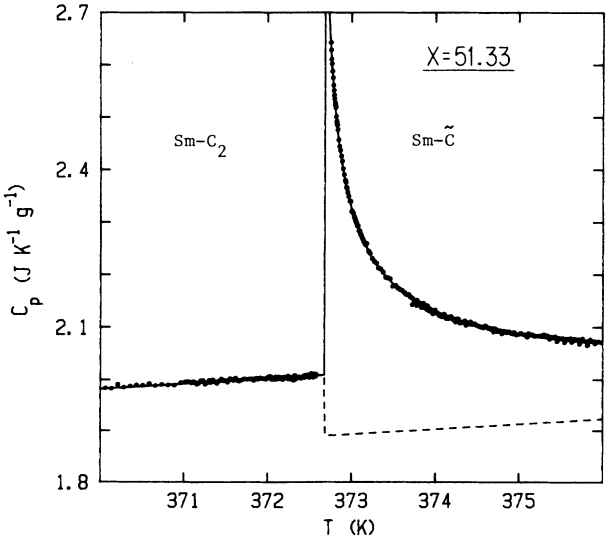

FIG. 11. Inverted Landau fit to the C_p variation associated with the Sm-$\tilde{C}$–Sm-C_2 transition in the 51.33 mol % mixture. Data points obtained in the first-order coexistence region are not shown and were not used in the fit. Fit parameters are given in Table I.

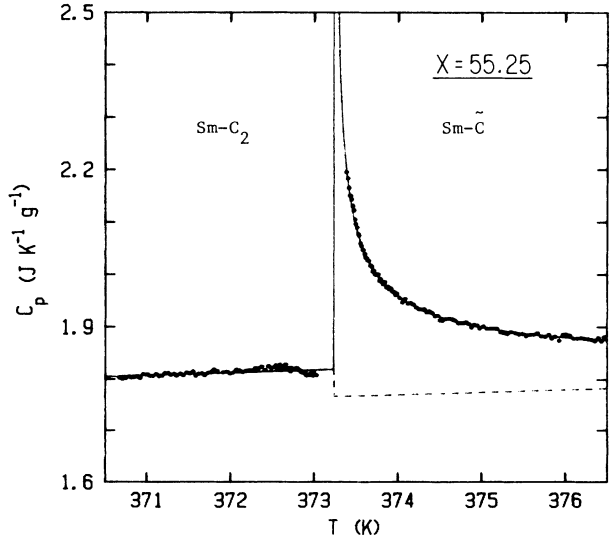

FIG. 12. Inverted Landau fit to the C_p variation associated with the Sm-$\tilde{C}$–Sm-C_2 transition in the 55.25 mol % mixture. Data points obtained in the first-order coexistence region are not shown and were not used in the fit. Fit parameters are given in Table I.

TABLE I. Parameters obtained from a least-squares fit of Sm-$\tilde{C}$–Sm-C_2 heat-capacity data with Eq. (2). The value of T_1 can be taken to be any temperature in the coexistence region that lies above T_k; we have chosen $T_1 = T_k + 0.04$ K for the plots shown in Figs. 11 and 12.

X (mol %)	T_1 (K)	T_k (K)	A^* ($J K^{-1/2} g^{-1}$)	ΔC_p ($J K^{-1} g^{-1}$)	B ($J K^{-1} g^{-1}$)	$10^3 E$ ($J K^{-2} g^{-1}$)	χ_ν^2
51.33	372.669	372.629	0.265	0.119	1.890	9.96	0.98
55.25	373.279	373.239	0.164	0.054	1.766	5.30	3.61[a]

[a]This large χ_ν^2 value is completely due to the small nonlinearity of C_p in the Sm-C_2 phase between 372 and 373 K; see Fig. 12.

In summary, there are two aspects of the C_p variation associated with a Sm-$\tilde{C}$–Sm-C_2 transition: a large inverted Landau variation in the Sm-$\tilde{C}$ phase, which is due to polarization ordering in a Sm-A-like mass-density structure, and a small step increase due to the molecular axis tilt. The magnitudes of ΔC_p given in Table I are small compared to the C_p step size (0.55 $J K^{-1} g^{-1}$) observed at the second-order Sm-A_2–Sm-C_2 transition in DB_8ClCN (octylphenyl-chloro-cyanobenzoyloxy benzoate).[20] The mean-field character of the polarization ordering seems reasonable since the polarization interactions in the Sm-$\tilde{C}$ structure must be long range. Also the absence of any extended critical behavior for C_p in the Sm-C_2 phase is expected since the phase is fully ordered when it "locks in".[1,2]

Sm-A_1–Sm-$\tilde{C}$ transition. The Sm-A_1–Sm-$\tilde{C}$ transition is a rare case of a smectic-A to smectic-C transition that is first order. This is theoretically predicted to be so because of Brazovskii fluctuations.[2] As shown in Fig. 6, the asymmetric excess heat-capacity peak at $T_{A_1\text{-}\tilde{C}}$ roughly resembles the type of mean-field behavior observed at Sm-A–Sm-C transition in nonpolar compounds.[21] However, the Landau model that works well for nonpolar Sm-A–Sm-C transitions does not provide an adequate description of our Sm-A_1–Sm-$\tilde{C}$ data. This is not surprising in view of the Sm-$\tilde{C}$ structure shown in Fig. 10. The closest analogy for the Sm-A_1–Sm-$\tilde{C}$ transition is the Sm-A_1–Sm-$\tilde{A}$ transition. In the latter case, the heat capacity exhibits a mean-field-like feature below the weakly first-order transition plus a very broad pretransitional excess C_p that extends ~ 10 K above the transition.[22] In the present system, excess heat capacity associated with the Sm-A_1–Sm-$\tilde{C}$ transition definitely exists over a range of ~ 3 K below the transition and may well exist over a wider range and in the high-temperature Sm-A_1 phase also. It is difficult to make a precise evaluation since the Sm-A_1–Sm-$\tilde{C}$ peak lies close to a large N_r–Sm-A_1 peak. The background curves shown in Figs. 2, 3, and 6 represent our estimates of upper and lower bounds for the tail of the $C_p(N_r\text{–Sm-}A_1)$ peak. The $\Delta C_p(N_r\text{–Sm-}A_1)$ fit described below for the 51.33 mol % sample seems to support the choice of the lower background curve, but this is very tentative since a considerable extrapolation beyond the fitting range is required. Even if the lower background curves are correct, the excess C_p for the Sm-A_1–Sm-$\tilde{C}$ transition in $DB_8ONO_2 + DB_{10}ONO_2$ is smaller above the transition than that for the Sm-A_1–Sm-$\tilde{A}$ transition[22] in $DB_nCN + C_5$stilbene (by a factor of ~ 2).

The Sm-A_1–Sm-$\tilde{C}$ excess heat capacity is in good qualitative agreement with x-ray results on DB_9ONO_2 (Ref. 11) and $DB_8ONO_2 + DB_{10}ONO_2$ mixtures.[23] In DB_9ONO_2, Sm-$\tilde{C}$-like fluctuations are observed in the Sm-A_1 phase but they are weaker than Sm-$\tilde{A}$ fluctuations seen in the Sm-A_1 phase near the Sm-A_1–Sm-$\tilde{A}$ transition in closely related systems.[11,13] Over a range of ~ 3 K just below the Sm-A_1–Sm-$\tilde{C}$ transition, the x-ray scattering is anomalous and does not show the resolution-limited Sm-$\tilde{C}$ peaks seen at lower temperatures. Instead, the x-ray pattern shows strong and broad Sm-A_1-like diffuse scattering at $q_2 = 2\pi/L$ and diffuse Sm-$\tilde{C}$-like scattering at $q_{1z} \simeq 0.65 q_2$.[11] The excess heat capacity over a range of a few degrees below $T_{A_1\text{-}\tilde{C}}$ represents energy changes associated with the development of long-range Sm-$\tilde{C}$ polarization modulation. However, the Sm-$\tilde{C}$ phase in this region is quite imperfect in both polarization and mass-density order (almost nematic in character).

Sm-A_d–N_r–Sm-A_1 region. Only the 51.33 mol % sample showed both a Sm-A_d–N_r and N_r–Sm-A_1 heat-capacity peak. The relative size of these two peaks, shown in Fig. 7, agrees qualitatively with expectations based on the frustrated spin-gas model and experimental results on T8 (octyloxybenzyloxy cyanostilbene).[16] The Sm-A_d–N_r peak is smaller than that in T8, and the Sm-A_d fluctuations in the N_r phase are very large.[23] Almost all the energy effects in this region are associated with short-range dipolar interactions that change only on going into the Sm-A_1 phase.

The N_r–Sm-A_1 peak for this 51.33 mol % sample was large and stable. Thus it was possible to carry out an analysis of this peak with the critical fluctuation form

$$C_p^{\pm} = A^{\pm}|t|^{-\alpha}(1 + D_1^{\pm}|t|^{\Delta_1} + D_2^{\pm}|t|^{2\Delta_1}) + B + E(T - T_c), \quad (6)$$

where the reduced temperature $t = (T - T_c)/T_c$ and the superscripts $\pm$ denote above and below T_c. The corrections-to-scaling exponent Δ_1 is taken to be 0.5, and a second corrections-to-scaling term is included since the analysis of N–Sm-A_1 transitions has shown this to play a significant role.[24] The minimum and maximum reduced temperatures for the 51.33 mol % data set are $t_{\min} = +3.7\times10^{-5}$ and -9.0×10^{-5}, $t_{\max} = +1.2\times10^{-3}$ ($T < 399.6$ K to avoid the Sm-A_d–N_r peak) and -4.1×10^{-3} ($T > 397.5$ K to avoid possible systematic errors due to any pretransitional excess heat capacity associated with the Sm-A_1–Sm-$\tilde{C}$ transition). Since the total fitting range is only 2.1 K, the slope E was set equal to

zero.

Preliminary fits with Eq. (6) yielded α values close to the tricritical value of 0.5 rather than the XY value of -0.007 obtained for second-order N–Sm-A_1 transitions in other samples.[24] In this case, the correction term $A^{\pm}D_1^{\pm}|t|^{\Delta_1-\alpha}$ becomes a temperature-independent term that can have different values above and below T_c.[25] Thus we will rewrite Eq. (6) in the tricritical form

$$C_p^{\pm}=A^{\pm}|t|^{-0.5}(1+D_2^{\pm}|t|)+B^{\pm} . \quad (7)$$

Good fits of Eq. (7) to the 51.33 mol% C_p data were obtained with $B^+\neq B^-$ ($\chi_\nu^2=1.03$) and with the constraint $B^+=B^-$ imposed ($\chi_\nu^2=1.04$); see Fig. 13. The least-squares values of the parameters were $T_c=399.141$ K, $A^+=5.40\times10^{-3}$, $A^-/A^+=1.546$, $D_2^+=131.1$, $D_2^-/D_2^+=(1)$, $B^+=1.970$, $B^-=2.002$; and $T_c=399.142$ K, $A^+=5.12\times10^{-3}$, $A^-/A^+=1.658$, $D_2^+=46.14$, $D_2^-/D_2^+=3.04$, $B^+=B^-=1.992$. The units for $A^{\pm}$ and $B^{\pm}$ are $\mathrm{J\,K^{-1}\,g^{-1}}$, and parentheses indicate that the ratio D_2^-/D_2^+ was held fixed at the given value for the first fit. The values of χ_ν^2 and the fitting parameters were stable when $t_{\max}$ in the Sm-A_1 phase was changed from -4.1×10^{-3} to either -1.2×10^{-3} or -7.9×10^{-3}. Thus we conclude that the N_r–Sm-A_1 tricritical composition is at or very near 51.33 mol% $DB_{10}ONO_2$.[26] It should be noted that the (nonuniversal) N–Sm-A_1 tricritical amplitude ratio A^-/A^+ agrees very well with that reported for the N–Sm-A_m tricritical point in nonpolar 40.8+60.8 mixtures rather than that for the N–Sm-A_d tricritical point in polar 8CB+10CB mixtures; see Ref. 25 for a discussion of nonuniversal tricritical ratios.

On the basis of the above discussion, one would expect that mixtures with $51.33<X<X^*$, where X^* denotes the composition at the Sm-A_d–N_r–Sm-A_1 point, should exhibit first-order N_r–Sm-A_1 transitions. The present data are consistent with this idea but not definitive due to the thermal instability of the N_r–Sm-A_1 peaks for samples with $X=53.2$, 54.2, 55.0, and 55.25. The best support is provided by the data on the 54.2 mol% sample. The initial run on this sample showed that two data points (omitted from Fig. 8) near the transition exhibited large phase shifts ϕ, indicating a 56-mK two-phase coexistence region. A fit with Eq. (6) to the 54.2 mol% data shown in Fig. 8 yields a fit with $\chi_\nu^2=4.8$ and an effective critical exponent $\alpha_{\mathrm{eff}}=0.56$. Such effective α values greater than $\frac{1}{2}$ are usually obtained on fitting a weakly first-order transition peak.[25] Thus the tricritical point must lie somewhere in the interval $51.3<X_{\mathrm{TCP}}<54.2$.

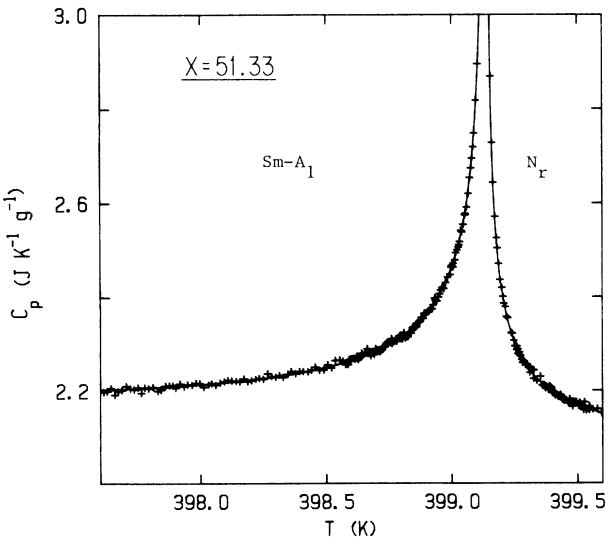

FIG. 13. Fit of the N_r–Sm-A_1 heat-capacity peak for the 51.33 mol% mixture. The solid curve represents Eq. (7) using the parameters given in the text for the fit with the scaling constraint $B^+=B^-$ imposed.

Additional support for the N_r–Sm-A_1 transition becoming first order before the nematic phase disappears is provided by the slow time evolution shown in Fig. 9 for the heat capacity of the 51.33 mol% sample. Brief periods at temperatures above 400 K (2 h prior to run 3) did not change the character of the N_r–Sm-A_1 or Sm-A_d–N_r transitions or greatly change the nematic range. However, prolonged periods above 400 K (86 h prior to run 4 and 193 h prior to run 7) cause the nematic range to decrease and drive the N_r–Sm-A_1 transition weakly first order.

The present experimental results in the Sm-A_d–N_r–Sm-A_1 region are qualitatively consistent with the microscopic and DSC results of Raja *et al.*[14] The DSC data suggested that a N_r–Sm-A_1 tricritical point exists in the $X=52$–53.5 range. The ac calorimetric data locate this tricritical point in the 51.33–54.2 mol% range and probably close to $X=51.33$. The high-resolution microscope data[14] yield an unusual phase topology near the Sm-A_d–N_r–Sm-A_1 point. Unfortunately, the scan rates required by the ac calorimeter (or any other high-resolution technique) are intrinsically slow and the phase transitions near the Sm-A_d–N_r–Sm-A_1 point are very sensitive to small quantities of thermally generated impurities. As a result, the behavior of the Sm-A_d–N_r and N_r–Sm-A_1 phase transition lines near the Sm-A_d–N_r–Sm-A_1 point could not be well determined. Our best estimates of the transition temperatures in the Sm-A_d–N_r–Sm-A_1 region are given in Fig. 4(b). There is general qualitative agreement with the high-resolution phase diagram of Raja *et al.*,[14] but there are differences in both temperatures and compositions. Note that our estimated composition at the Sm-A_d–N_r–Sm-A_1 point ($X^*\simeq56$) is 1 mol% larger than that reported in Ref. 14. Small shifts in transition temperatures and X^* are almost certainly due to small differences in the purity of the samples. The DB_8ONO_2 and $DB_{10}ONO_2$ starting materials used to prepare the present mixtures were not the same as those used in Ref. 14. In addition to these shifts in X^* and the transition temperatures for the Sm-A_d–N_r–Sm-A_1 region, the Sm-A_2 phase is missing in our mixtures. Both these features are very sensitive to impurities.

Although impurities must be responsible for the difficulties described above, it should be stressed that the

Sm-A_d–N_r and N_r–Sm-A_1 transitions are extremely sensitive to impurities when X is close to X^*. We do not believe that the impurity level is very high in any of the samples; note that the Sm-A_1–Sm-$\tilde{C}$ and Sm-$\tilde{C}$–Sm-C_2 transition temperatures are stable over long periods at high temperature even when the N_r–Sm-A_1 transition has shifted by as much as 3 K. This sensitivity of the Sm-A_d–N_r–Sm-A_1 transition behavior to impurities when X is near X^* is reflected in the frustrated spin-gas model[7] by a dramatic sensitivity of the Sm-A_1-phase stability to the model parameters when these parameter values are close to those required to realize the phase sequence seen near X^*. The role of thermally generated impurities can also be seen in the behavior of the Sm-A_d–N_r and N_r–Sm-A_1 heat-capacity peaks shown in Fig. 9.

IV. SUMMARY

Binary mixtures of the homologs DB_8ONO_2 and $DB_{10}ONO_2$ exhibit complex phase behavior in the vicinity of the Sm-A_d–N_r–Sm-A_1 point at $X^* \simeq 56$. The excess heat capacity associated with the Sm-A_d–N_r transition is much smaller than that at the N_r–Sm-A_1 transition. The N_r–Sm-A_1 transition exhibits tricritical behavior at $X_{TCP} \simeq 51.3$ and becomes first order in the range $X_{TCP} < X < X^*$. This supports the proposal of Raja *et al.*[14] that the Sm-A_d–N_r–Sm-A_1 multicritical point is a Sm-A_d–N_r critical end point that lies close to a tricritical point on the N_r–Sm-A_1 line. It is clear, however, that the complex behavior of the Sm-A_d–N_r and N_r–Sm-A_1 phase lines as they approach the Sm-A_d–N_r–Sm-A_1 point is not yet well characterized experimentally or understood theoretically. Theoretical extensions of the multiply reentrant frustrated spin-gas model[7] and the nematic-bubble model[27] seem promising in this regard. Experimental work would be greatly enhanced by the discovery of more stable systems, especially since very high sensitivity to impurities seems to be an intrinsic feature of this region.

All the investigated samples exhibit the Sm-A_1–Sm-$\tilde{C}$–Sm-C_2 phase sequence at slightly lower temperatures. The Sm-A_1–Sm-$\tilde{C}$ transition is weakly first order, and the C_p anomaly resembles that seen at Sm-A_1–Sm-$\tilde{A}$ transitions. However, the excess heat capacity above the transition, due to Sm-$\tilde{C}$ fluctuations in the Sm-A_1 phase, is much smaller than that associated with Sm-$\tilde{A}$ fluctuations in Sm-A_1 near Sm-A_1–Sm-$\tilde{A}$ transitions. No Sm-A_2 phase was observed for these samples. The direct Sm-C–Sm-$\tilde{C}_2$ transition is a weakly first-order transition with a large excess data capacity in the Sm-$\tilde{C}$ phase that can be very well described by an inverted Landau model; no pretransitional thermal behavior was observed in the Sm-C_2 phase.

ACKNOWLEDGMENTS

We wish to thank G. Heppke for providing samples of DB_8ONO_2 and $DB_{10}ONO_2$ and J. D. Litster for the use of his polarizing microscope. We also wish to thank P. A. Heiney, A. M. Levelut, and C. R. Safinya for helpful discussions. This work was supported by the National Science Foundation under Grant No. DMR-87-02052.

*Present address: Department of Physics, Tokyo Institute of Technology, Oh-Okayama, Meguro, Tokyo 152, Japan.

[1]J. Prost, J. Phys. (Paris) **40**, 581 (1979); in *Liquid Crystals of One- and Two-Dimensional Order*, edited by W. Helfrich and G. Heppke (Springer-Verlag, Berlin, 1980), p. 125.

[2]J. Prost and P. Barois, J. Chim. Phys. **80**, 65 (1983); J. Prost, Adv. Phys. **33**, 1 (1984).

[3]P. Barois, J. Prost, and T. C. Lubensky, J. Phys. (Paris) **46**, 391 (1985).

[4]J. Prost (private communication).

[5]A. N. Berker and J. S. Walker, Phys. Rev. Lett. **47**, 1469 (1981).

[6]J. O. Indekeu and A. N. Berker, Phys. Rev. A **33**, 1158 (1986).

[7]J. O. Indekeu, Phys. Rev. A **37**, 288 (1988); J. O. Indekeu and A. N. Berker, J. Phys. (Paris) **49**, 353 (1988).

[8]F. Hardouin, A. M. Levelut, M. F. Achard, and G. Sigaud, J. Chim. Phys. **80**, 53 (1983).

[9]N. H. Tinh, F. Hardouin, and C. Destrade, J. Phys. (Paris) **43**, 1127 (1982).

[10]R. Shashidhar, B. R. Ratna, V. Surendranath, V. N. Raja, S. Krishna Prasad, and C. Nagabhusan, J. Phys. (Paris) Lett. **46**, L-445 (1985).

[11]E. Fontes, P. A. Heiney, J. L. Haseltine, and A. B. Smith, J. Phys. (Paris) **47**, 1533 (1986).

[12]R. Shashidhar (unpublished).

[13]F. Hardouin, N. H. Tinh, M. F. Achard, and A. M. Levelut, J. Phys. (Paris) Lett. **43**, L-327 (1982); C. R. Safinya, W. A. Varady, L. Y. Chiang, and P. Dimon, Phys. Rev. Lett. **57**, 432 (1986).

[14]V. N. Raja, R. Shashidhar, B. R. Ratna, G. Heppke, and Ch. Bahr, Phys. Rev. A **37**, 303 (1988).

[15]K. W. Evans-Lutterrodt, J. W. Chung, B. M. Ocko, R. J. Birgeneau, C. Chiang, C. W. Garland, E. Chin, J. Goodby, and N. H. Tinh, Phys. Rev. A **36**, 1387 (1987).

[16]J. O. Indekeu, A. N. Berker, C. Chiang, and C. W. Garland, Phys. Rev. A **35**, 1371 (1987).

[17]C. W. Garland, Thermochim. Acta **88**, 127 (1985); K. J. Stine, Ph.D. thesis, Massachusetts Institute of Technology, 1988 (unpublished).

[18]R. Shashidhar, K. A. Suresh, B. R. Ratna, S. Krishna Prasad, Ch. Bahr, A. Gobl-Wunsch, and G. Heppke, Mol. Cryst. Liq. Cryst. Lett. **1**, 89 (1985).

[19]C. W. Garland and M. E. Huster, Phys. Rev. A **35**, 2365 (1987).

[20]Y. H. Jeong, K. J. Stine, and C. W. Garland, Phys. Rev. A **37**, 3465 (1988).

[21]M. Meichle and C. W. Garland, Phys. Rev. A **27**, 2624 (1983).

[22]K. Ema, C. W. Garland, G. Sigaud, and N. H. Tinh, Phys. Rev. A **39**, 1369 (1989).

[23]R. Shashidhar and B. R. Ratna (unpublished).

[24]C. W. Garland, G. Nounesis, and K. J. Stine (unpublished).
[25]K. J. Stine and C. W. Garland, Phys. Rev. A (to be published).
[26]It should be noted that the McMillan ratio $T_{N\text{-}A}/T_{N\text{-}I}$ equals 0.80 at this tricritical point, but this ratio is not a significant variable in the present situation. Indeed, the value of $T_{N\text{-}A}/T_{N\text{-}I}$ is almost independent of X along the N–Sm-A_1 line.
[27]J. Prost and J. Toner, Phys. Rev. A **36**, 5008 (1987).